Title

H2BZmacropa-NCS: A Bifunctional Chelator for Actinium-225 Targeted Alpha Therapy.

Journal

Bioconjugate Chemistry, 33(6)

Authors

Kadassery, Karthika

King, A

Fayn, Stanley

et al.

Publication Date

2022-06-15

DOI

10.1021/acs.bioconjchem.2c00190

Peer reviewed

HHS Public Access

Author manuscript

Bioconjug Chem. Author manuscript; available in PMC 2022 August 09.

Published in final edited form as:

Bioconjug Chem. 2022 June 15; 33(6): 1222–1231. doi:10.1021/acs.bioconjchem.2c00190.

H_2BZmacropa-NCS: A Bifunctional Chelator for Actinium-225 Targeted Alpha Therapy

Karthika J. Kadassery[§,†], **A. Paden King**[§,‡], **Stanley Fayn**[‡], **Kwamena E. Baidoo**[‡], **Samantha N. MacMillan**[†], **Freddy E. Escorcia**[‡,*], **Justin J. Wilson**[†,**]

[†]Department of Chemistry and Chemical Biology, Cornell University, Ithaca, New York 14853, United States.

[‡]Center for Cancer Research, National Cancer Institute, National Institutes of Health, Bethesda, Maryland 20892, United States.

Abstract

Actinium-225 (^{225}Ac) is one of the most promising radionuclides for targeted alpha therapy (TAT). With a half-life of 9.92 days and a decay chain that emits four high energy α particles, ^{225}Ac is well-suited for TAT when conjugated to macromolecular targeting vectors that exhibit extended in vivo circulation times. The implementation of ^{225}Ac in these targeted constructs, however, requires a suitable chelator that can bind and retain this radionuclide in vivo. Previous work has demonstrated the suitability of a diaza-18-crown-6 macrocyclic chelator H_2macropa for this application. Building upon these prior efforts, in this study, two rigid variants of H_2macropa, which contain either one (H_2BZmacropa) or two (H_2BZ_2macropa) benzene rings within the macrocyclic core, were synthesized and investigated for their potential use for ^{225}Ac TAT. The coordination chemistry of these ligands with La^{3+}, used as a non-radioactive model for Ac^{3+}, was carried out. Both NMR spectroscopic and X-ray crystallographic studies of the La^{3+} complexes of these ligands revealed similar structural features as those found for the related complex of H_2macropa. Thermodynamic stability constants of the La^{3+} complexes, however, were found to be one and two orders of magnitude lower than those of H_2macropa for H_2BZmacropa and H_2BZ_2macropa, respectively. The decrease in thermodynamic stability was rationalized via the use of density functional theory calculations. ^{225}Ac radiolabeling and serum stability studies with H_2BZmacropa showed that this chelator compares favorably with H_2macropa. Based on these promising results, a bifunctional version of this chelator, H_2BZmacropa-NCS, was synthesized and conjugated to the antibody codrituzumab (GC33), which targets the liver cancer biomarker glypican-3 (GPC3). The resulting GC33-BZmacropa conjugate and an analogous GC33-macropa were evaluated for their ^{225}Ac radiolabeling efficiencies, antigen-binding affinity, and in vivo

[*]Freddy Escorcia, 10 Center Drive, Building 10, Room 1B54, Bethesda, Maryland 20892, (240) 858-3062, freddy.escorcia@nih.gov.
[**]Justin Wilson, G50A Baker Laboratory, Cornell University, Ithaca, New York 14853, (607) 255-4344, jjw275@cornell.edu.
[§]Denotes Equally Contributing Authors

JJW and KJK are co-inventors on a provisional patent application on the use of the chelators reported in this manuscript for targeted alpha therapy applications.

Supporting Information

The Supporting Information is available free of charge on the ACS Publications website.

Synthetic procedures, experimental details, and supplementary figures. (PDF)

X-ray crystal data (CIF)

DFT optimized geometries (ZIP)

biodistribution in HepG2 liver cancer tumor-bearing mice. Although both conjugates were comparably effective in their radiolabeling efficiencies, [^{225}Ac]Ac-GC33-BZmacropa showed slightly poorer serum stability and biodistribution than [^{225}Ac]Ac-GC33-macropa. Together, these results establish H_2BZmacropa-NCS as a new bifunctional chelator for the preparation of ^{225}Ac radiopharmaceuticals.

Graphical Abstract

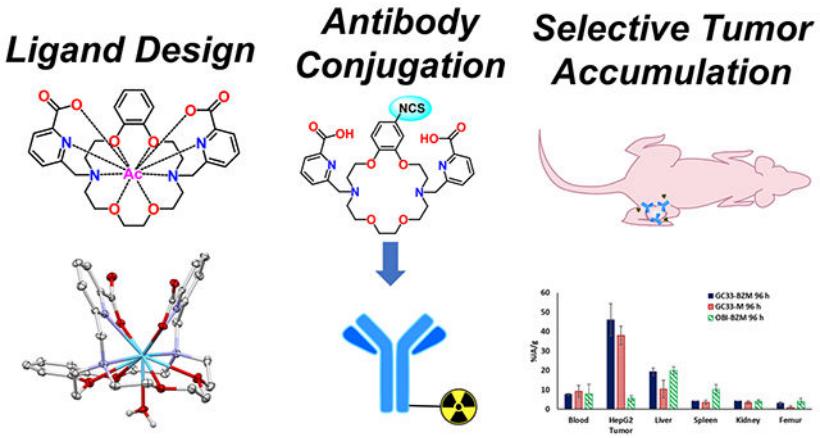

Introduction

The 2013 FDA approval of $^{223}RaCl_2$ (Xofigo®) for the management of bone metastases in castration-resistant prostate cancer (mCRPC) patients has heralded a renaissance in targeted alpha therapy (TAT), a treatment modality that uses the high linear energy transfer of alpha (α) particles to annihilate cancer cells.[1] Despite the success of this drug, the development of new radiopharmaceutical agents employing ^{223}Ra has been hindered by the difficult chelation chemistry of this ion.[2] Fortunately, a number of other α-emitting radionuclides, such as ^{227}Th, ^{225}Ac, ^{213}Bi, ^{212}Bi, ^{212}Pb, and ^{211}At, have suitable properties for use in TAT.[3] Among these radionuclides, ^{225}Ac has demonstrated particular promise due to advances in its large-scale production, its ideal 9.92-day physical half-life for conjugation to long-lived biomolecules, and high cytotoxic potency, which arises from the four α particles emitted through its decay chain.[4,5] Clinical trials of ^{225}Ac small-molecule[6,7] and antibody[8] conjugates are underway, and early results have been promising.

A significant limitation in the development of new ^{225}Ac-based TAT radiopharmaceutical agents has arisen from the difficulty in identifying suitable chelating agents for the large Ac^{3+} ion.[5] Although acyclic chelators such as ethylenediamine tetraacetic acid (H_4EDTA) and diethylenetriamine pentaacetic acid (H_5DTPA) have been shown to possess high affinity for the $^{225}Ac^{3+}$ ion, the resulting complexes are labile, leading to release of the free metal ion in biological systems.[9] By contrast, many Ac^{3+} complexes of macrocyclic chelators are substantially more inert. For example, the macrocyclic chelator tetraazacyclododecane-1,4,7,10-tetraacetic acid (H_4DOTA) has been used successfully for both small molecule and antibody ^{225}Ac-radioconjugates, albeit with some significant challenges. For example, radiolabeling of H_4DOTA with ^{225}Ac either requires high

temperature, which are incompatible with macromolecular biomolecules like antibodies, or long incubation times, which yields constructs with relatively low-specific-activities.[10-14] Furthermore, serum stability studies have shown that the ^{225}Ac]Ac-DOTA complex dissociates over time,[15] a property that is corroborated by animal studies that show deposition of ^{225}Ac in the liver and femur after the administration of DOTA-based conjugates.[16] These drawbacks have sparked efforts to develop superior bifunctional chelators for ^{225}Ac.

To accommodate the large ionic radius of Ac^{3+}, researchers have targeted alternative ligands that contain greater than 8 donor atoms to saturate its coordination sphere. For instance, the macrocycles bispa,[17] crown,[18] macrodipa, and py-macrodipa[19] as well as the acyclic chelators octapa,[15] py4pa[20] and phospha[15] have all successfully radiolabeled $^{225}Ac^{3+}$ at room temperature in < 60 min. However, not all these chelators form sufficiently stable complexes with ^{225}Ac for biological use.

Among the potential alternative to H_4DOTA, the diaza-18-crown-6 macrocyclic chelator H_2macropa (Chart 1) has shown significant promise for ^{225}Ac chelation in TAT applications.[24,25] This compound is unique by virtue of its high selectivity for large over small lanthanide ions,[21] a property that makes it favorable for use with the large Ac^{3+} ion. In contrast to H_4DOTA, this chelator can quantitatively radiolabel ^{225}Ac at room temperature in 5 mins and form complexes that are sufficiently stable for long-term biological applications. The success of this chelator for use with ^{225}Ac has been demonstrated by several studies that have used it in conjunction with small-molecule and antibody-based targeting vectors.[26-29]

The efficacy of H_2macropa suggests that this structural archetype is valuable for Ac^{3+} chelation. Building upon this scaffold, two new analogues of H_2macropa were investigated. These compounds are rigidified versions of the parent chelator, containing either one (H_2BZmacropa) or two (H_2BZ_2macropa) benzene rings within the 18-membered macrocycle (Chart 1). We hypothesized that the decreased conformational flexibility of these new analogues would preorganize them for more effective and stable chelation of the Ac^{3+} ion.[30-35] This study presents a comprehensive comparative investigation of these new chelators with respect to their La^{3+} and Ac^{3+}-complexing properties. Furthermore, a bifunctional chelator, H_2BZmacropa-NCS, and its conjugate to the glypican-3 (GPC3)-targeting antibody codrituzumab[36] (GC33) were prepared. The resulting ^{225}Ac-labeled GC33-BZmacropa conjugate was then assessed in an in vivo mouse model of liver cancer. Collectively, the results from this study highlight the importance of ligand design principles in developing effective chelating agents for TAT applications.

RESULTS AND DISCUSSION

Chelate Syntheses.

The previously reported ligands, H_2macropa[21] and H_2BZmacropa,[37] and the novel ligand H_2BZ_2macropa were synthesized via adaptations of procedures that have been used to access related macrocyclic chelators.[38] Briefly, the ligands were synthesized by the alkylation of the corresponding diaza-18-crown-6 macrocycle at the secondary amine

nitrogen with 6-(bromomethyl)pyridine-2-carboxylic acid methyl ester followed by acid hydrolysis of the ester functional groups (Scheme S1-S2). The ligands were fully characterized by NMR spectroscopy, mass spectrometry, elemental analysis, and analytical HPLC (Figures S1-S29).

Coordination Chemistry with La^{3+}.

Because no stable isotopes of Ac^{3+} exist, the coordination chemistries of H_2BZmacropa and H_2BZ_2macropa were investigated using La^{3+}. As the largest lanthanide, this ion has a similar ionic radius, hydrolysis constant, and hard-soft acid-base properties to Ac^{3+}, thus rendering it a suitable model.[5,39] Treatment of equimolar ratios of $LaCl_3$ with each compound in water at neutral pH followed by salt metathesis with KPF_6 led to the precipitation of the $[LaL(H_2O)]PF_6$ complexes, which were crystallized via the slow evaporation of concentrated aqueous solutions at room temperature. The structures of these complexes (Figure 1), as determined by X-ray crystallography, are comparable to that of $[La(macropa)(H_2O)]^+$.[24] In all three complexes, the La^{3+} center attains an 11-coordinate geometry with 10 donors provided by the macrocyclic ligands and the 11th arising from an inner-sphere water molecule that interpenetrates the macrocyclic core.

Within the macropa^{2-} and BZmacropa^{2-} structures, the metal ion sits above the mean plane of the O-atoms in the macrocycle (O1—O4), resulting in near linear N1—La—N2 angles of 178.04° and 172.41°, respectively. By contrast, the structure of $[La(BZ_2macropa)(H_2O)]^+$ shows that all the donor atoms of the macrocyclic base reside in a plane below the La^{3+} center, rendering the N1—La—N2 angle to be much more acute (148.77°). This distortion is most likely a consequence of the presence of the two rigid benzene groups, which lead to additional strain in the macrocycle of BZ_2macropa^{2-} upon coordination to the La^{3+} backbone.

In addition to this distortion, there are also significant differences with respect to the interatomic distances between the donor atoms and the La^{3+} center within these structures. For example, the inner coordination sphere of the La^{3+} ion in the BZmacropa complex is relatively asymmetric; the La—N distances on the macrocycle are 2.857 and 2.957 Å, representing a significant difference of 0.1 Å. Furthermore, the La—O distances from the aryl ether oxygens of the macrocycle are significantly disparate at 2.772 and 3.058 Å. By contrast, the crystal structure of $[La(BZ_2macropa)(H_2O)]^+$ is relatively symmetric with chemically equivalent donor atoms interacting with the La^{3+} center at similar distances. However, the La—O distances within the macrocycle fall between 2.83 and 2.96 Å. By contrast, the crystal structure of $[La(macropa)]^+$ has La—O distances that are much shorter (between 2.70 and 2.79 Å). Thus, the aryl ethers donors conferred by the benzene ring appear to interact more weakly than the aliphatic ethereal donors, as evidenced by the longer interatomic distances in the former.

Solution Thermodynamics with La^{3+}.

To assess the effects of the presence of the rigid benzene groups on the metal-binding properties of H_2BZmacropa and H_2BZ_2macropa, the thermodynamic stabilities of their La^{3+} complexes were measured via pH potentiometric titrations. The protonation constants of

H_2BZmacropa and H_2BZ_2macropa and the stability constants of their La^{3+} complexes are collected in Table 1. For both the chelators, a total of four protonation constants were observed over a pH range of 2.5–11.3. The first and the second protonation constants most likely correspond to the sequential protonation of the macrocyclic amine nitrogen atoms, whereas the third and the fourth protonation constants are assigned to the protonation at the picolinate pendent arms. Although there are six basic sites on the chelators, the fifth and sixth protonation constants could not be determined using the pH ranges employed in these titrations. The sum of the first and second protonation constants of the rigid compounds are 0.8 and 1.3 log units, respectively, lower than that of macropa, indicating that the addition of phenyl groups increases the acidity of the macrocycles. This result is an expected consequence of the electron-withdrawing nature of the phenyl groups and is consistent with previously reported data on similar macrocyclic chelators.[40-42] It should be noted that the protonation constants for H_2BZmacropa have been previously reported,[37] and these values—in particular the most basic protonation constant—differ somewhat from those measured in this study. The use of different media for ionic strength (0.1 M KCl vs 0.1 M KNO_3) could partly explain these discrepancies. In any case, the pH potentiometric titrations in the present study were carried out in triplicate and are reported with a high degree of confidence.

After obtaining the protonation constants, the La^{3+} stability constants (log K_{LaL}) of the H_2BZmacropa and H_2BZ_2macropa complexes were determined by pH potentiometric titrations (Table 1). The log K_{LaL} values decrease upon the addition of phenyl groups to the macrocyclic backbone, following the sequence log $K_{Lamacropa}$ > log $K_{LaBZmacropa}$ > log $K_{LaBZ2macropa}$. The stability constant for the La^{3+} complex of H_2BZmacropa (log K_{LaL} = 13.99) is approximately 1 log unit lower than that of H_2macropa (log K_{LaL} = 14.99). The introduction of a second phenyl group in H_2BZ_2macropa leads to an even greater destabilization of the complexes, as reflected by log K_{LaL} (log K_{LaL} = 12.04) that is almost 2 log units lower than that of H_2BZmacropa. In order to account for the effect of protonation equilibria of the ligands on complex stability, the conditional stability constants (log K'_{LaL}) and pLa (the negative log of the free metal concentration in a solution containing 10^{-6} M metal ion and 10^{-5} M chelator) at biologically relevant pH = 7.4 were calculated (Table 1). The trends in these conditional stability constants follow those of the absolute values with log $K'_{Lamacropa}$ = 14.63, log $K'_{LaBZmacropa}$ = 13.81, and log $K'_{LaBZ2macropa}$ = 11.92. Although ligand rigidification should in principle lead to enhanced metal complex stability, this effect may depend on several factors including the type of metal employed. For example, a previous study of ethylene glycol-bis(β-aminoethyl ether)-N,N,N′,N′-tetraacetic acid (H_4EGTA) and an analogue of H_4EGTA with a phenyl backbone showed that enhanced stability was exhibited for the Ca^{2+} complex, but stability decreased for the La^{3+} complex.[42] The reduced stability observed in the cases of H_2BZmacropa and H_2BZ_2macropa may thus be a consequence of several different factors.

Although the overall LaL stability constants for the rigid ligands are lower than that of H_2macropa, the absolute values exceed 10, suggesting that they form sufficiently strong complexes for use in ^{225}Ac TAT.

DFT Calculations.

In order to better understand the La^{3+} stability constant trends, density functional theory (DFT) was employed. The geometries of $[La(macropa)(OH_2)]^+$, $[La(BZmacropa)(OH_2)]^+$, and $[La(BZ_2macropa)(OH_2)]^+$ were first optimized. The resulting structures are qualitatively similar to the experimentally determined X-ray crystal structures, but exhibit a systematic elongation of the La donor atom distances within the macrocycles of approximately 0.05–0.10 Å. More importantly, however, the relatively asymmetry of $[La(BZmacropa)(OH_2)]^+$ is captured by the DFT optimization, thus validating this level of theory. With suitably optimized structures, the $\Delta G°$ values for the transchelation reaction between $[La(macropa)(H_2O)]^+$ and either $BZmacropa^{2-}$ or $BZ_2macropa^{2-}$ were calculated.

$$[La(macropa)(H_2O)]^+ + BZmacropa^{2-} \rightarrow [La(BZmacropa)(H_2O)]^+ + macropa^{2-} \qquad \Delta G^\circ = 7.03 \text{ kJ/mol}$$

$$[La(macropa)(H_2O)]^+ + BZ_2macropa^{2-} \rightarrow [La(BZ_2macropa)(H_2O)]^+ + macropa^{2-} \qquad \Delta G^\circ = 16.8 \text{ kJ/mol}$$

For both of these reactions, the $\Delta G°$ was found to be > 0, indicating that both $BZmacropa^{2-}$ and $BZ_2macropa^{2-}$ form less thermodynamically stable complexes with La^{3+} than $macropa^{2-}$. Furthermore, $\Delta G°$ for the transchelation with $BZ_2macropa^{2-}$ was approximately 10 kJ/mol greater than that for $BZmacropa^{2-}$. Collectively, these computational results are consistent with our experimental data that show $BZ_2macropa^{2-}$ forms the least stable La^{3+} complex of these three ligands.

Having validated our computational method against the experimental results, we analyzed the different factors that contribute to $\Delta G°$ for these reactions. As described in the Supporting Information (Section S1.6), $\Delta G°$ can be expressed as the sum $\Delta\Delta G_S° + \Delta\Delta G_B°$, where $\Delta\Delta G_S°$ is the relative ligand strain energy and $\Delta\Delta G_B°$ is the relative metal ion-binding energy (see SI section S1.6 for more details).[35,38,43,44] The strain energy ($\Delta G_S°$) is defined as the free energy change required to distort the geometrically relaxed free ligand (L) to a conformation that is suitable for metal ion-binding (L_{strain}, eq. S1), and the binding energy ($\Delta G_B°$) is defined as the free energy change associated with the incorporation of the La^{3+} ion into the ligand in its preorganized metal-binding conformation (eq. S2). The relative ($\Delta\Delta G$) values, compared to $macropa^{2-}$, are given below.

$$\Delta\Delta G_S^\circ(BZmacropa^{2-}) = -13.95 \text{ kJ/mol}$$
$$\Delta\Delta G_B^\circ(BZmacropa^{2-}) = 20.98 \text{ kJ/mol}$$

$$\Delta\Delta G_S^\circ (BZ_2macropa^{2-}) = -14.41\ kJ/mol$$
$$\Delta\Delta G_B^\circ (BZ_2macropa^{2-}) = 31.17\ kJ/mol$$

For both BZmacropa^{2-} and BZ$_2$macropa^{2-} $\Delta\Delta G_S°$ are negative, indicating that these compounds undergo a significantly smaller free energy penalty for attaining an appropriate metal-binding conformation than macropa^{2-}. This result is consistent with role of the rigid benzene groups in enhancing the metal-binding preorganization of these ligands. By contrast, the $\Delta\Delta G_B°$ values for both rigid chelators are positive, a result that suggests that macropa forms stronger binding interactions with the La^{3+} ion. The weaker binding energies of H$_2$BZmacropa and H$_2$BZ$_2$macropa, compared to H$_2$macropa, is most likely a consequence of their decreased basicity and donor strength. As noted above, the electron-withdrawing phenyl groups embedded in the macrocycle decreases their basicity, as determined experimentally via protonation constant measurements. This decreased basicity also renders them less effective Lewis bases for binding with La^{3+}. To further verify this conclusion computationally, the $\Delta G°$ for a simple model ligand substitution reaction on La^{3+} was calculated. In this substitution reaction, the $\Delta G°$ values required to displace dimethyl ether, a model for the aliphatic ether donors in H$_2$macropa, with anisole, an aromatic ether that models the donors on H$_2$BZmacropa and H$_2$BZ$_2$macropa. These calculations revealed that displacement of dimethyl ether by anisole is thermodynamically uphill ($\Delta G°$ = 17.22 kJ/mol). Thus, the weaker donor strengths of the aromatic ethers is a plausible explanation for the positive $\Delta\Delta G_B°$ determined for H$_2$BZmacropa and H$_2$BZ$_2$macropa. Together, these results reveal a counterbalancing effect of the introduction of the rigid phenyl groups. Although these rigid phenyl groups provide a favorable entropic contribution by preorganizing the ligands for metal binding, their weaker donor strengths provide a poorer enthalpic contribution to La^{3+} binding. For BZmacropa^{2-} and BZ$_2$macropa^{2-}, the weaker binding strength outweighs the benefits obtained in ligand preorganization.

Radiolabeling and Stability Studies.

With the comprehensive characterization of the La^{3+} complexes of BZmacropa^{2-} and BZ$_2$macropa^{2-}, which revealed them to be effective ligands for this ion, their ability to chelate Ac^{3+} was investigated. The chelators (~300 μM) were incubated at room temperature with 70 μCi (2.6 Mbq) [^{225}Ac]Ac(NO$_3$)$_3$ in water containing NH$_4$OAc (0.1 M) at pH 5.5. Under these conditions, both ligands, as well as macropa, quantitatively radiolabeled $^{225}Ac^{3+}$ in only 30 min, resulting in high specific activities of approximately 7.5 Ci/g (260 TBq/g). Instant thin-layer chromatography (ITLC) chromatograms, showing the complex formation for these ligands and macropa, are in the Supporting Information, Figures S63-S66. These results, particularly the room temperature radiolabeling, confirm the high efficacy of expanded macrocyclic ligands like macropa^{2-} for chelation of the large Ac^{3+} ion.

Having demonstrated the rapid and high specific activity radiolabeling with H$_2$BZmacropa and H$_2$BZ$_2$macropa, the stabilities of the resulting Ac^{3+} complexes in whole human serum at 37°C were evaluated (Figure 2, S70-S72). Under these conditions, all complexes were >90% intact after 5 days. Even with this high uniform stability among the complexes several trends could be discerned. Specifically, increasing stability of the complexes followed the

order $BZ_2macropa^{2-}$ < $BZmacropa^{2-}$ < $macropa^{2-}$. This trend matches that observed with the thermodynamic stability constant data of the La^{3+} complexes that was rationalized with DFT calculations, described above.

Bifunctional Chelator, H_2BZmacropa-NCS.

The high stability of the ^{225}Ac complex of BZmacropa prompted us to prepare a bifunctional version of this chelator. For this purpose, we targeted the chelator H_2BZmacropa-NCS (Chart 1), which contains an amine-reactive isothiocyanate group appended to the phenyl ring of the macrocyclic backbone. The synthesis of this compound (Scheme 1) commenced from the macrocycle **3** which upon treatment with 1 equiv. of KNO_3 in trifluoracetic acid afforded the monosubstituted nitro-product **8** in near quantitative yield. The addition of the pendent arms to the nitrated macrocycle was accomplished by alkylation of **8** at the secondary amine nitrogen with 6-(bromomethyl)pyridine-2-carboxylic acid methyl ester. Reduction of the nitrated compound **9** using H_2 over Pd/C followed by acid hydrolysis of the ester functional groups yielded H_2BZmacrcopa-NH_2. Finally, the isothiocyanate functional group was installed onto the macrocycle via the treatment of H_2BZmacrcopa-NH_2 with excess thiophosgene. The compound H_2BZmacrcopa-NCS was fully characterized by NMR spectroscopy, mass spectrometry, and analytical HPLC (Figures S30-S40).

A key difference between the first-generation bifunctional chelator H_2macropa-NCS (Chart 1) and H_2BZmacropa-NCS is the location of the amine-reactive –NCS group. On H_2BZmacropa-NCS, this functional group is attached to the macrocycle backbone, whereas for H_2macropa-NCS it is on one of the picolinate pendent arms. Consequently, the synthesis of the H_2BZmacropa-NCS is more modular in that it proceeds through intermediate **8**, which can potentially be functionalized with a diverse range of different pendent donor arms to access a library of different bifunctional chelators. Furthermore, the H_2BZmacropa-NCS is relatively easier to synthesize as compared to H_2macropa-NCS. For instance, the synthesis of H_2macropa-NCS involves a 9-step pathway starting from the macrocycle, while the synthesis of H_2BZmacropa-NCS is carried out in 4–5 steps. The location of the –NCS functional group also has important effects on its hydrolytic stability. For instance, a solution of H_2macropa-NCS in pH 9.1 $NaHCO_3$ buffer at room temperature completely hydrolyzes to the amine H_2macropa-NH_2 in approximately 5 h ($t_{1/2}$ = 1.25 h). Under the same conditions, the hydrolysis of H_2BZmacropa is significantly slower ($t_{1/2}$ = 56 h), requiring over a week for near complete formation of the amine. The location of the –NCS group of H_2macropa-NCS directly on the electron-deficient picolinate group increases its electrophilicity, rendering it more reactive and less stable than the –NCS group of H_2BZmacropa-NCS that is linked to a more electron-rich phenyl group. The increased stability of H_2BZmacropa-NCS marks a potential advantage over H_2macropa-NCS, for H_2BZmacropa-NCS may be shipped at room temperature and stored for extended periods of time, rendering it more broadly accessible to researchers across the globe.

Antibody Conjugation.

To further evaluate the suitability of H_2BZmacropa-NCS as a bifunctional chelator, this compound was conjugated to the antibody GC33, which targets the GPC3 receptor

overexpressed in many liver cancers. The H_2BZmacropa-NCS conjugate of GC33 (GC33-BZM) was prepared using standard antibody-isothiocyanate coupling conditions, which use a slight molar excess (2.5–3 equiv.) of chelator exposed to the antibody in bicarbonate buffer at 37 °C. These conditions were also applied to prepare the macropa conjugate of GC33 (GC33-M) and the H_2BZmacropa-NCS conjugate of Obinutuzumab (OBI-BZM), an antibody that does not bind GPC3. The conjugates were subjected to gel-permeation chromatography to remove any unconjugated bifunctional chelator, and their purities were verified by size-exclusion HPLC (Figures S52-S54).

After purification, the average chelator:antibody ratios were determined. Previous studies have shown that presence of too many covalently attached chelators on antibodies can have negative consequences on their immunoreactivity and pharmacokinetic properties. As such, a chelator:antibody ratio of <5 is generally desirable for radioconjugates.[45-47] The chelator:antibody ratios were assessed using a modification of the previously reported colorimetric arsenazo assay (Figures S58-S59).[48] All conjugates were found to have chelator:antibody ratios of approximately 1:1 using this method, indicating that minimal alteration of the antibody was achieved. To provide further verification of these results, the chelator:antibody ratios of GC33-M and GC33-BZM were also determined using UPLC-HRMS. The resulting mass spectra, shown in Figures S55-S57, correspond well with the chelate:antibody ratios determined using the arsenazo method.

Having established the degree of functionalization of these conjugates, we next investigated the impact of this modification on the immunoreactivity of GC33 using bio-layer interferometry (BLI). The exposure of various concentrations of antibody-chelator conjugates to immobilized GPC3 antigen revealed concentration-dependent binding of the antibody to the surface and subsequent dissociation. The combined association and dissociation kinetic data across all concentrations were fit using the global fitting model in the Octet Analysis Studio software (Figures S60-S62). These data revealed K_d values of 0.19, 0.14, and 0.042 nM for GC33-BZM, GC33-M, and GC33 respectively. Taken together, the results show that both GC33-BZM and GC33-M retained comparably high binding affinity for GPC3 that was slightly diminished relative to the free GC33 antibody.

Radiolabeling and Stability Studies with Chelator-Antibody Conjugates.

After confirming the identity, purity, and antigen-binding affinity of the antibody conjugates, they were radiolabeled with ^{225}Ac following a previously reported procedure that was used for GC33-M.[29] Under these conditions, a solution of antibody conjugates (450 μg) was added to a solution of ^{225}Ac (150 μCi, 5.55 MBq) in aqueous 0.1 M NH_4OAc (pH 5.5). The mixtures were incubated at room temperature for 30 min, after which the completion of the radiolabeling was checked with ITLC (Condition 2). Purification of the radioconjugates by gel permeation chromatography afforded them in >95% purity, as verified by ITLC (Condition 2) (Figures S67-S69). The mild conditions and rapid reaction time required for these radiolabelings highlight the suitability of these chelators for antibody radioconjugates of ^{225}Ac. Importantly, the rapid room temperature radiolabeling afforded by these conjugates is critical for minimizing radiolytic damage and thermal aggregation or denaturation of the antibody.

The stabilities of [^{225}Ac]Ac-GC33-BZM and [^{225}Ac]Ac-GC33-M were evaluated in whole human serum at 37°C over several days (Figure 3, S73-S74). Radio-ITLC analysis (Condition 2) revealed that [^{225}Ac]Ac-GC33-M remained > 90% intact over 7 days, highlighting the excellent stability of the ^{225}Ac complex of the bifunctional macropa-NCS^{2-} chelator. By contrast, the radioconjugate [^{225}Ac]Ac-GC33-BZM exhibited marked degradation over the course of the experiment, with approximately 55% intact complex remaining after 7 days. The reduced stability of the [^{225}Ac]Ac-GC33-BZM conjugate relative to the unconjugated ligand-^{225}Ac complex, which showed good stability in human serum, may arise from the electron-withdrawing effect of the thiourea moiety on the ligand backbone, which decreases the donating capacity of the ligand. Notably, for both GC33-M and GC33-BZM radioconjugates, ITLC traces revealed the presence of 3 distinct species in solution: intact conjugate, “free” ^{225}Ac chelated by the mobile phase EDTA, and a third unknown species. This third species reached approximately 10% of the total activity over the course of 1 day, then remained constant throughout the experiment. We hypothesize that this unknown product may be [^{225}Ac]Ac-macropa or [^{225}Ac]Ac-BZmacropa that has been cleaved from the antibody by radiolysis of the thiourea linker, for extensive radiolysis is often observed in solutions containing ^{225}Ac.[18,49]

Biodistribution Studies.

Despite the lower stability of the [^{225}Ac]Ac-GC33-BZM conjugate relative to [^{225}Ac]Ac-GC33-M, we hypothesized that the former may still have sufficient stability for tumor targeting in vivo. To test whether [^{225}Ac]Ac-GC33-BZM could successfully target GPC3+ tumors in vivo, we treated athymic nude mice bearing HepG2 (GPC3+) xenografts with 100 nCi (3.7 kBq) of [^{225}Ac]Ac-GC33-BZM, ^{225}Ac[Ac]-GC33-M (positive control), and [^{225}Ac]Ac-OBI-BZM (isotype control). After 48 and 96 h, mice (n = 3–4) were euthanized, and their organs were weighed and counted using a gamma counter after allowing 24 h for daughter isotope equilibration. The % injected-activity per gram (IA/g) in each organ was then calculated (Figure 4, S75-S77). As expected, the isotype control [^{225}Ac]Ac-OBI-BZM, which does not target the GPC3+ liver cancer xenografts, showed no appreciable tumor uptake at any time point. By contrast, [^{225}Ac]Ac-GC33-BZM demonstrated clear, specific tumor uptake at both 48 and 96 h post-injection, with tumor signal greater than that of all organs at both time points. Importantly, the tumor uptake of [^{225}Ac]Ac-GC33-BZM was effectively indistinguishable from that of ^{225}Ac[Ac]-GC33-M, indicating that these conjugates have comparable targeting capability. “However, the off-target accumulation of ^{225}Ac in both the liver and femur was higher after administration of [^{225}Ac]Ac-GC33-BZM than for ^{225}Ac[Ac]-GC33-M.” A similar degree of liver uptake was also observed in the non-targeted isotype control conjugate [^{225}Ac]Ac-GC33-BZM. Unchelated ^{225}Ac has previously been shown to localize to the liver almost exclusively. Therefore, the higher liver uptake measured for both [^{225}Ac]Ac-GC33-BZM and [^{225}Ac]Ac-OBI-BZM may be a consequence of partial instability of [^{225}Ac]Ac-BZmacropa complex under these conditions.[9] Despite these drawbacks, [^{225}Ac]Ac-GC33-BZM still demonstrates significant tumor uptake, suggesting that BZmacropa-NCS may be viable as a bifunctional chelator for in vivo studies of ^{225}Ac-labeled antibody conjugates.

CONCLUSION

In summary, two rigid variants of the first-generation ^{225}Ac chelator H_2macropa were synthesized by incorporating either one or two benzene rings into the macrocyclic base. Our comprehensive coordination chemistry studies of these ligands with La^{3+}, a non-radioactive surrogate for Ac^{3+}, revealed that they form complexes of lower stability than H_2macropa. DFT calculations were used to show that the use of phenyl groups in the backbone enhances their preorganization at the cost of their overall enthalpy of metal binding. These results highlight the different factors that need to be taken into consideration in designing and optimizing chelators for nuclear medicine applications. Despite their lower thermodynamic stability with La^{3+}, ^{225}Ac-radiolabeling studies with these ligands proceeded effectively, yielding high specific activity compounds within minutes at room temperature. Thus, these chelators are among the few candidates that can bind ^{225}Ac under such mild conditions, rendering them valuable for use with sensitive macromolecular targeting vectors.

Based on these promising results, the bifunctional variant H_2BZmacropa-NCS was synthesized. In contrast to other large macrocyclic bifunctional chelators for ^{225}Ac, H_2BZmacropa-NCS places the reactive functional group directly on the macrocycle rather than the pendent arms. This design difference has two important implications. First, the synthetic approach is modular in that it allows for the installation of different pendent donor groups without perturbing the functional group handle on the macrocycle. Second, the stability of the –NCS functional group is substantially enhanced relative to that of the first-generation macropa-NCS. For this first-generation analogue, the –NCS group is installed on the pendent picolinate group and hydrolyzes rapidly both in the solid and solution state. These latter properties have made shipping and storage of this compound challenging. The enhanced hydrolytic stability of H_2BZmacropa-NCS, by contrast, should make it more accessible to other researchers. To further evaluate the suitability of this new bifunctional chelator, it was conjugated to the antibody GC33, which can be employed for targeting liver cancers that express GPC3. Consistent with our expectations based on the small-molecule chelators, radiolabeling of the GC33-BZM proceeded rapidly under mild, room temperature conditions. However, our serum stability and biodistribution studies revealed the ^{225}Ac-labeled GC33-BZM to be less stable than the macropa conjugate, yet still capable of delivering this radionuclide to the tumor site. Although the serum and in vivo stability of the ^{225}Ac-labeled GC33-BZM present some concerns, further optimization of this new bifunctional chelator, via modification of either the pendent donor arms or extension of the linker between the reactive –NCS group and the aromatic ring, may afford complexes of enhanced stability suitable for further clinical development. Alternatively, the use of H_2BZmacropa-NCS for other promising α-emitting radionuclides also warrants investigation. These efforts are currently underway within our labs.

Supplementary Material

Refer to Web version on PubMed Central for supplementary material.

ACKNOWLEDGMENT

A.P.K., S.F., K.E.B, and F.E.E acknowledge the support from Intramural Research Program funds ZIA BC 011800 and ZIA BC 010891. K.J.K. and J.J.W. were supported by Department of Energy Basic Energy Sciences (award No. DE-SC0021662) and National Institutes of Biomedical Imaging and Bioengineering of the National Institutes of Health (award numbers R21EB027282 and R01EB02925). J.J.W also acknowledge the support from Research Corporation for Science Advancement through a Cottrell Research Scholar Award. We are grateful to Chugai Pharmaceutical for providing codrituzumab (GC33).

REFERENCES

(1). Parker C; Nilsson S; Heinrich D; Helle SI; O'Sullivan JM; Fosså SD; Chodacki A; Wiechno P; Logue J; Seke M; et al. Alpha Emitter Radium-223 and Survival in Metastatic Prostate Cancer. N. Engl. J. Med 2013, 369 (3), 213–223. [PubMed: 23863050]

(2). Abou DS; Thiele NA; Gutsche NT; Villmer A; Zhang H; Woods JJ; Baidoo KE; Escorcia FE; Wilson JJ; Thorek DLJ Towards the Stable Chelation of Radium for Biomedical Applications with an 18-Membered Macrocyclic Ligand. Chem. Sci 2021, 12 (10), 3733–3742. [PubMed: 34163647]

(3). Nelson BJB; Andersson JD; Wuest F Targeted Alpha Therapy: Progress in Radionuclide Production, Radiochemistry, and Applications. Pharmaceutics 2021, 13 (1), 49.

(4). King AP; Lin FI; Escorcia FE Why Bother with Alpha Particles? Eur. J. Nucl. Med. Mol. Imaging 2021, 49 (1), 7–17. [PubMed: 34175980]

(5). Thiele NA; Wilson JJ Actinium-225 for Targeted α Therapy: Coordination Chemistry and Current Chelation Approaches. Cancer Biother. Radiopharm 2018, 33 (8), 336–348. [PubMed: 29889562]

(6). Yadav MP; Ballal S; Sahoo RK; Tripathi M; Seth A; Bal C Efficacy and Safety of ^{225}Ac-PSMA-617 Targeted Alpha Therapy in Metastatic Castration-Resistant Prostate Cancer Patients. Theranostics 2020, 10 (20), 9364–9377. [PubMed: 32802197]

(7). Ballal S; Yadav MP; Bal C; Sahoo RK; Tripathi M Broadening Horizons with ^{225}Ac-DOTATATE Targeted Alpha Therapy for Gastroenteropancreatic Neuroendocrine Tumour Patients Stable or Refractory to ^{177}Lu-DOTATATE PRRT: First Clinical Experience on the Efficacy and Safety. Eur. J. Nucl. Med. Mol. Imaging 2020, 47 (4), 934–946. [PubMed: 31707430]

(8). Tagawa ST; Sun M; Sartor AO; Thomas C; Singh S; Bissassar M; Fernandez E; Niaz MJ; Ho B; Vallabhajosula S et al. Phase I Study of ^{225}Ac-J591 for Men with Metastatic Castration-Resistant Prostate Cancer (MCRPC). J. Clin. Oncol 2021, 39 (15_suppl), 5015–5015.

(9). Davis IA; Glowienka KA; Boll RA; Deal KA; Brechbiel MW; Stabin M; Bochsler PN; Mirzadeh S; Kennel SJ Comparison of ^{225}Actinium Chelates: Tissue Distribution and Radiotoxicity. Nucl. Med. Biol 1999, 26 (5), 581–589. [PubMed: 10473198]

(10). Maguire WF; McDevitt MR; Smith-Jones PM; Scheinberg DA Efficient 1-Step Radiolabeling of Monoclonal Antibodies to High Specific Activity with ^{225}Ac for α-Particle Radioimmunotherapy of Cancer. J. Nucl. Med 2014, 55 (9), 1492–1498. [PubMed: 24982438]

(11). Mesude B; Katharina L; Teja K; Phelps ME; Strand S; Morris MJ; Radu CG; Damoiseaux R; Peltola MT; Peekhaus N; et al. Genetic Signature of Prostate Cancer Mouse Models Resistant to Optimized HK2 Targeted α-Particle Therapy. Proc. Natl. Acad. Sci 2020, 117 (26), 15172–15181. [PubMed: 32532924]

(12). Lakes AL; An DD; Gauny SS; Ansoborlo C; Liang BH; Rees JA; McKnight KD; Karsunky H; Abergel RJ Evaluating ^{225}Ac and ^{177}Lu Radioimmunoconjugates against Antibody–Drug Conjugates for Small-Cell Lung Cancer. Mol. Pharm 2020, 17 (11), 4270–4279. [PubMed: 33044830]

(13). Sudo H; Tsuji AB; Sugyo A; Kaneko MK; Kato Y; Nagatsu K; Suzuki H; Higashi T Preclinical Evaluation of Podoplanin-Targeted Alpha-Radioimmunotherapy with the Novel Antibody NZ-16 for Malignant Mesothelioma. Cells 2021, 10 (10), 2503. [PubMed: 34685483]

(14). Sudo H; Tsuji AB; Sugyo A; Harada Y; Nagayama S; Katagiri T; Nakamura Y; Higashi T FZD10-Targeted α-Radioimmunotherapy with ^{225}Ac-Labeled OTSA101 Achieves Complete

Remission in a Synovial Sarcoma Model. Cancer Sci. 2022, 113 (2), 721–732. [PubMed: 34935247]

(15). Ramogida CF; Robertson AKH; Jermilova U; Zhang C; Yang H; Kunz P; Lassen J; Bratanovic I; Brown V; Southcott L; et al. Evaluation of Polydentate Picolinic Acid Chelating Ligands and an α-Melanocyte-Stimulating Hormone Derivative for Targeted Alpha Therapy Using ISOL-Produced ^{225}Ac. EJNMMI Radiopharm. Chem 2019, 4 (1), 21. [PubMed: 31659557]

(16). Deal KA; Davis IA; Mirzadeh S; Kennel SJ; Brechbiel MW Improved in Vivo Stability of Actinium-225 Macrocyclic Complexes. J. Med. Chem 1999, 42 (15), 2988–2992. [PubMed: 10425108]

(17). Comba P; Jermilova U; Orvig C; Patrick BO; Ramogida CF; Rück K; Schneider C; Starke M Octadentate Picolinic Acid-Based Bispidine Ligand for Radiometal Ions. Chem. Eur. J 2017, 23 (63), 15945–15956. [PubMed: 28815804]

(18). Yang H; Zhang C; Yuan Z; Rodriguez-Rodriguez C; Robertson A; Radchenko V; Perron R; Gendron D; Causey P; Gao F; et al. Synthesis and Evaluation of a Macrocyclic Actinium-225 Chelator, Quality Control and In Vivo Evaluation of ^{225}Ac-Crown-AMSH Peptide. Chem. Eur. J 2020, 26 (50), 11435–11440. [PubMed: 32588455]

(19). Hu A; Brown V; MacMillan SN; Radchenko V; Yang H; Wharton L; Ramogida CF; Wilson JJ Chelating the Alpha Therapy Radionuclides $^{225}Ac^{3+}$ and $^{213}Bi^{3+}$ with 18-Membered Macrocyclic Ligands Macrodipa and Py-Macrodipa. Inorg. Chem 2022, 61 (2), 801–806. [PubMed: 34965102]

(20). Li L; Rousseau J; de G.Jaraquemada-Peláez M; Wang X; Robertson A; Radchenko V; Schaffer P; Lin K-S; Bénard F; Orvig C ^{225}Ac-H_4Py4pa for Targeted Alpha Therapy. Bioconjug. Chem 2021, 32 (7), 1348–1363. [PubMed: 32216377]

(21). Roca-Sabio A; Mato-Iglesias M; Esteban-Gómez D; Tóth É; de Blas A; Platas-Iglesias C; Rodríguez-Blas T Macrocyclic Receptor Exhibiting Unprecedented Selectivity for Light Lanthanides. J. Am. Chem. Soc 2009, 131 (9), 3331–3341. [PubMed: 19256570]

(22). Clarke ET; Martell AE Stabilities of Trivalent Metal Ion Complexes of the Tetraacetate Derivatives of 12-, 13- and 14-Membered Tetraazamacrocycles. Inorg. Chim. Acta 1991, 190 (1), 37–46.

(23). Martell AE, Smith Robert M., Critical Stability Constants. Volume 1,; Plenum Press: New York; London, 1974.

(24). Thiele NA; Brown V; Kelly JM; Amor-Coarasa A; Jermilova U; MacMillan SN; Nikolopoulou A; Ponnala S; Ramogida CF; Robertson AKH; et al. An Eighteen-Membered Macrocyclic Ligand for Actinium-225 Targeted Alpha Therapy. Angew. Chem. Int. Ed 2017, 56 (46), 14712–14717.

(25). Hu A; Wilson JJ Advancing Chelation Strategies for Large Metal Ions for Nuclear Medicine Applications. Acc. Chem. Res 2022, 55 (6), 904–915. [PubMed: 35230803]

(26). Kelly JM; Amor-Coarasa A; Ponnala S; Nikolopoulou A; Williams C; Thiele NA; Schlyer D; Wilson JJ; DiMagno SG; Babich JW A Single Dose of ^{225}Ac-RPS-074 Induces a Complete Tumor Response in an LNCaP Xenograft Model. J. Nucl. Med 2019, 60 (5), 649–655. [PubMed: 30413660]

(27). Aluicio-Sarduy E; Thiele NA; Martin KE; Vaughn BA; Devaraj J; Olson AP; Barnhart TE; Wilson JJ; Boros E; Engle JW Establishing Radiolanthanum Chemistry for Targeted Nuclear Medicine Applications. Chem. Eur. J 2020, 26 (6), 1238–1242. [PubMed: 31743504]

(28). Reissig F; Bauer D; Zarschler K; Novy Z; Bendova K; Ludik M-C; Kopka K; Pietzsch H-J; Petrik M; Mamat C Towards Targeted Alpha Therapy with Actinium-225: Chelators for Mild Condition Radiolabeling and Targeting PSMA—A Proof of Concept Study. Cancers. 2021, 13 (8), 1974. [PubMed: 33923965]

(29). Bell MM; Gutsche NT; King AP; Baidoo KE; Kelada OJ; Choyke PL; Escorcia FE Glypican-3-Targeted Alpha Particle Therapy for Hepatocellular Carcinoma. Molecules 2021, 26 (1), 4.

(30). De Sousa AS; Croft GJB; Wagner CA; Michael JP; Hancock RD Effect of Cyclohexylene Bridges on the Metal Ion Size Based Selectivity of Ligands in Aqueous Solution. Inorg. Chem 1991, 30 (18), 3525–3529.

(31). Brechbiel MW; Gansow OA Synthesis of C-Functionalized Trans-Cyclohexyldiethylenetriaminepenta-Acetic Acids for Labelling of Monoclonal Antibodies with the Bismuth-212 α-Particle Emitter. J. Chem. Soc. Perkin Trans. 1 1992, 9, 1173–1178.

(32). Ferreirós-Martínez R; Esteban-Gómez D; Platas-Iglesias C; de Blas A; Rodríguez-Blas T Zn(II), Cd(II) and Pb(II) Complexation with Pyridinecarboxylate Containing Ligands. Dalt. Trans 2008, 42, 5754–5765.

(33). Ramogida CF; Cawthray JF; Boros E; Ferreira CL; Patrick BO; Adam MJ; Orvig C H_2*CHX*Dedpa and H_4*CHX*Octapa—Chiral Acyclic Chelating Ligands for $^{67/68}$Ga and ^{111}In Radiopharmaceuticals. Inorg. Chem 2015, 54 (4), 2017–2031. [PubMed: 25621728]

(34). Wang X; de G. Jaraquemada-Peláez M; Cao Y; Ingham A; Rodríguez-Rodríguez C; Pan J; Wang Y; Saatchi K; Häfeli UO; Lin K-S; et al. H_2*CHX*Hox: Rigid Cyclohexane-Reinforced Nonmacrocyclic Chelating Ligand for [$^{Nat/67/68}$Ga]Ga^{3+}. Inorg. Chem 2020, 59 (7), 4895–4908. [PubMed: 32175726]

(35). Hu A; Aluicio-Sarduy E; Brown V; MacMillan SN; Becker KV; Barnhart TE; Radchenko V; Ramogida CF; Engle JW; Wilson JJ Py-Macrodipa: A Janus Chelator Capable of Binding Medicinally Relevant Rare-Earth Radiometals of Disparate Sizes. J. Am. Chem. Soc 2021, 143 (27), 10429–10440. [PubMed: 34190542]

(36). Ishiguro T; Sugimoto M; Kinoshita Y; Miyazaki Y; Nakano K; Tsunoda H; Sugo I; Ohizumi I; Aburatani H; Hamakubo T; Kodama T; Tsuchiya M; Yamada-Okabe H Anti–Glypican 3 Antibody as a Potential Antitumor Agent for Human Liver Cancer. Cancer Res. 2008, 68 (23), 9832–9838. [PubMed: 19047163]

(37). Panchenko PA; Zubenko AD; Chernikova EY; Fedorov YV; Pashanova AV; Karnoukhova VA; Fedyanin IV; Fedorova OA Synthesis, Structure and Metal Ion Coordination of Novel Benzodiazamacrocyclic Ligands Bearing Pyridyl and Picolinate Pendant Side-Arms. New J. Chem 2019, 43 (38), 15072–15086.

(38). Thiele NA; Woods JJ; Wilson JJ Implementing F-Block Metal Ions in Medicine: Tuning the Size Selectivity of Expanded Macrocycles. Inorg. Chem 2019, 58 (16), 10483–10500. [PubMed: 31246017]

(39). Deblonde GJ-P; Zavarin M; Kersting AB The Coordination Properties and Ionic Radius of Actinium: A 120-Year-Old Enigma. Coord. Chem. Rev 2021, 446, 214130.

(40). Corbaux P; Spiess B; Arnaud F; Schwing MJ Complexing Properties of an N,N′-Methylated Diaza-Crown-Ether. Polyhedron 1985, 4 (8), 1471–1473.

(41). Fedorova O; Fedorov Y; Oshchepkov M Complexes of Di- and Triazacrown Ethers with Heavy Metal Ions in Water Solution. Electroanalysis 2012, 24 (8), 1739–1744.

(42). Tei L; Baranyai Z; Botta M; Piscopo L; Aime S; Giovenzana GB Synthesis and Solution Thermodynamic Study of Rigidified and Functionalised EGTA Derivatives. Org. Biomol. Chem 2008, 6 (13), 2361–2368. [PubMed: 18563270]

(43). Wilson JJ; Ferrier M; Radchenko V; Maassen JR; Engle JW; Batista ER; Martin RL; Nortier FM; Fassbender ME; John KD; et al. Evaluation of Nitrogen-Rich Macrocyclic Ligands for the Chelation of Therapeutic Bismuth Radioisotopes. Nucl. Med. Biol 2015, 42 (5), 428–438. [PubMed: 25684650]

(44). Hu A; MacMillan SN; Wilson JJ Macrocyclic Ligands with an Unprecedented Size-Selectivity Pattern for the Lanthanide Ions. J. Am. Chem. Soc 2020, 142 (31), 13500–13506. [PubMed: 32697907]

(45). Vosjan MJWD; Perk LR; Visser GWM; Budde M; Jurek P; Kiefer GE; van Dongen GAMS Conjugation and Radiolabeling of Monoclonal Antibodies with Zirconium-89 for PET Imaging Using the Bifunctional Chelate p-Isothiocyanatobenzyl-Desferrioxamine. Nat. Protoc 2010, 5 (4), 739–743. [PubMed: 20360768]

(46). Al-Ejeh F; Darby JM; Thierry B; Brown MP A Simplified Suite of Methods to Evaluate Chelator Conjugation of Antibodies: Effects on Hydrodynamic Radius and Biodistribution. Nucl. Med. Biol 2009, 36 (4), 395–402. [PubMed: 19423007]

(47). Sharma SK; Glaser JM; Edwards KJ; Khozeimeh Sarbisheh E; Salih AK; Lewis JS; Price EW A Systematic Evaluation of Antibody Modification and ^{89}Zr-Radiolabeling for Optimized Immuno-PET. Bioconjug. Chem 2021, 32 (7), 1177–1191. [PubMed: 32197571]

(48). Dadachova E; Chappell LL; Brechbiel MW Spectrophotometric Method for Determination of Bifunctional Macrocyclic Ligands in Macrocyclic Ligand–Protein Conjugates. Nucl. Med. Biol 1999, 26 (8), 977–982. [PubMed: 10708314]

(49). Hooijman EL; Chalashkan Y; Ling SW; Kahyargil FF; Segbers M; Bruchertseifer F; Morgenstern A; Seimbille Y; Koolen SLW; Brabander T; et al. Development of [^{225}Ac]Ac-PSMA-I&T for Targeted Alpha Therapy According to GMP Guidelines for Treatment of MCRPC. Pharmaceutics 2021, 13 (5), 715. [PubMed: 34068206]

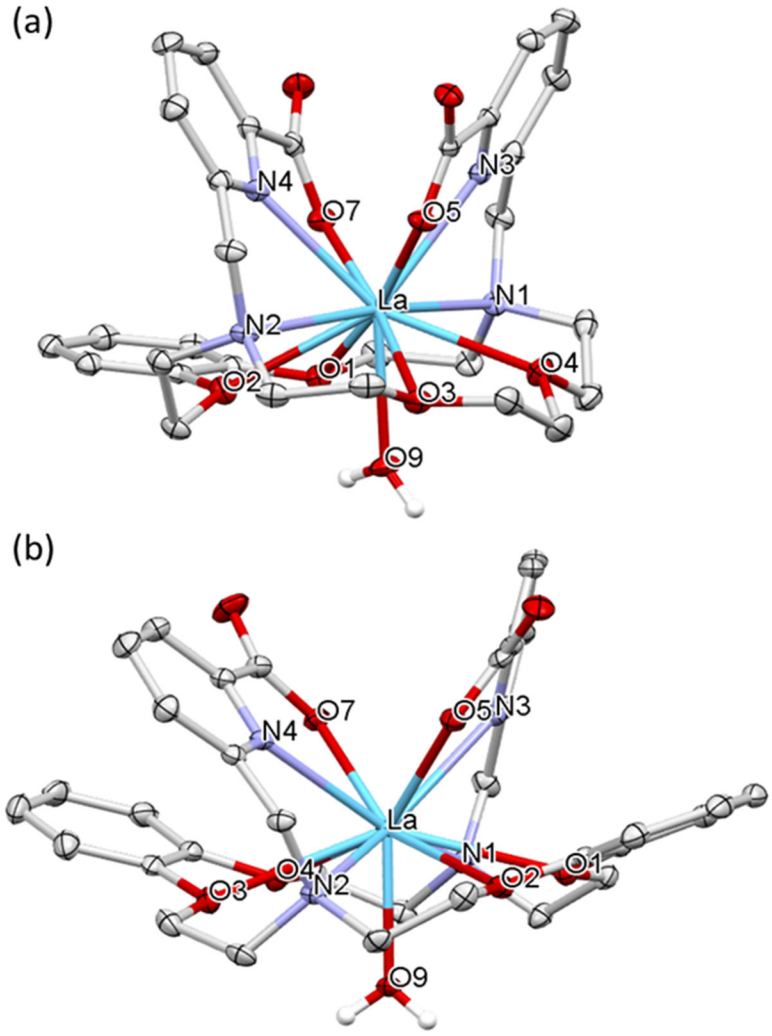

Figure 1.

Crystal structures of (a) [La(BZmacropa)(H_2O)](PF_6) and (b) [La(BZ_2macropa)(H_2O)](PF_6). Thermal ellipsoids are drawn at the 50% probability level. Outer-sphere solvents, counter-anions, and hydrogen atoms attached to carbon centers are omitted for clarity. Color scheme: La = blue; O = red; N = violet; C = grey.

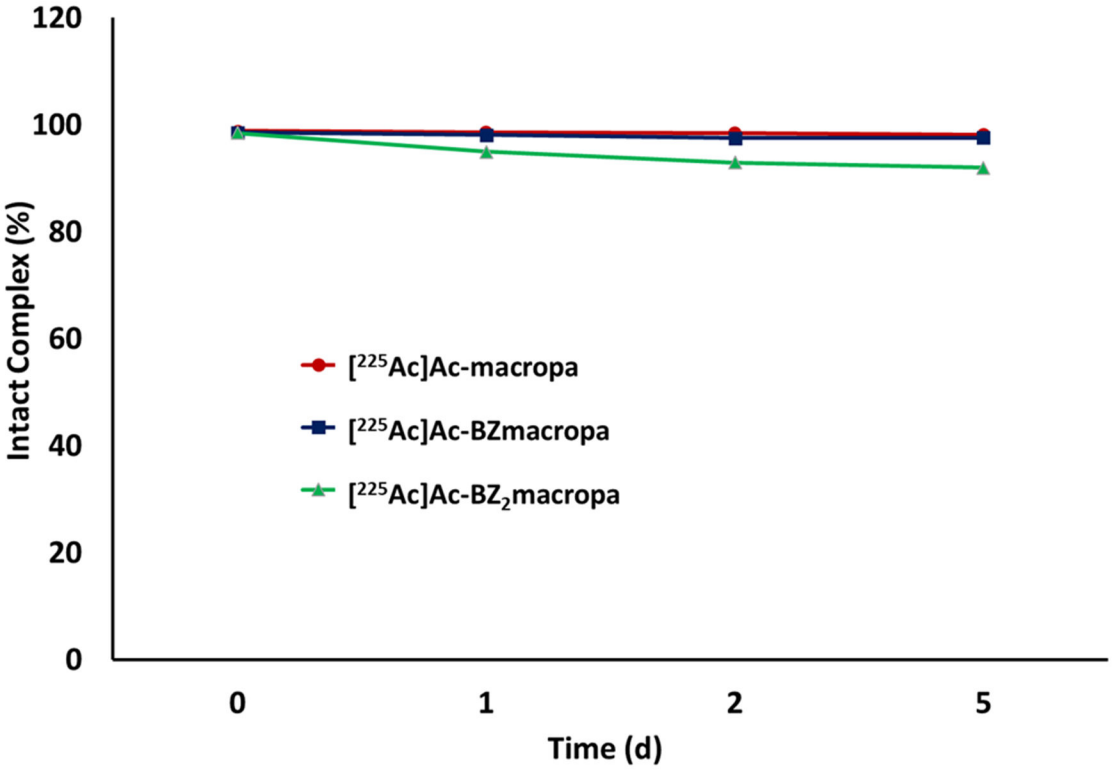

Figure 2.
Stability of ^{225}Ac complexes in human serum over time. Stability was measured using ITLC condition 1 as detailed in the Supporting Information.

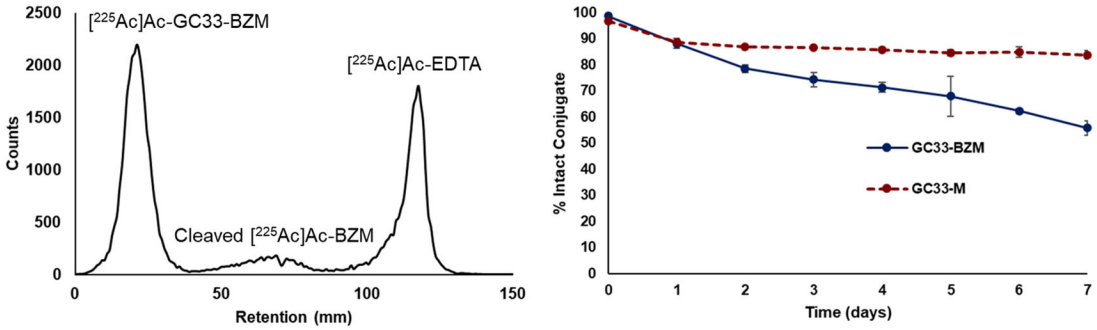

Figure 3.

(Left) ITLC chromatogram of [^{225}Ac]Ac-GC33-BZM after 7 day incubation in human serum at 37°C. (Right) Stability over time of [^{225}Ac]Ac-GC33-BZM and [^{225}Ac]Ac-GC33-M in human serum. Data points are the average of 3 independent samples and error bars represent the standard deviation.

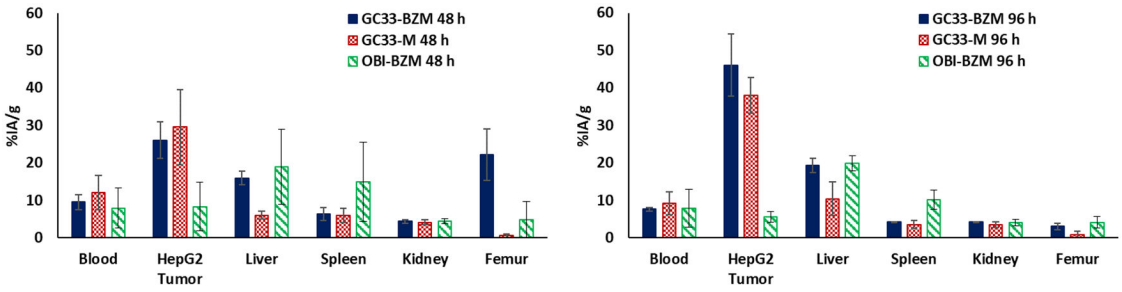

Figure 4.

Selected organ biodistribution of ^{225}Ac-labeled GC33-BZM (solid, blue bar), ^{225}Ac-labeled GC33-M (checkered, red bar), and ^{225}Ac-labeled OBI-BZM (striped, green bar) at 48 h (left panel) and 96 h (right panel) after administration (n = 3–4). Full biodistribution data can be found in the SI, Figures S58-S60.

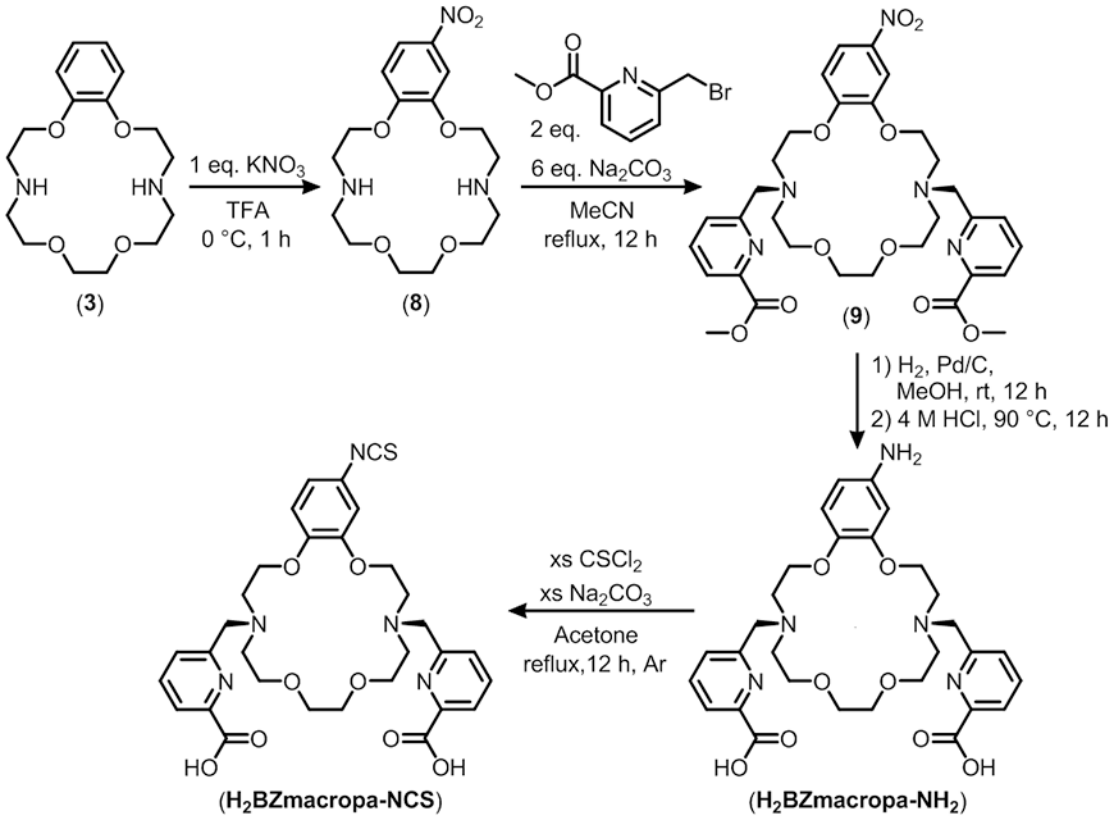

Scheme 1.
Synthetic scheme for H_2BZmacrop-NCS.

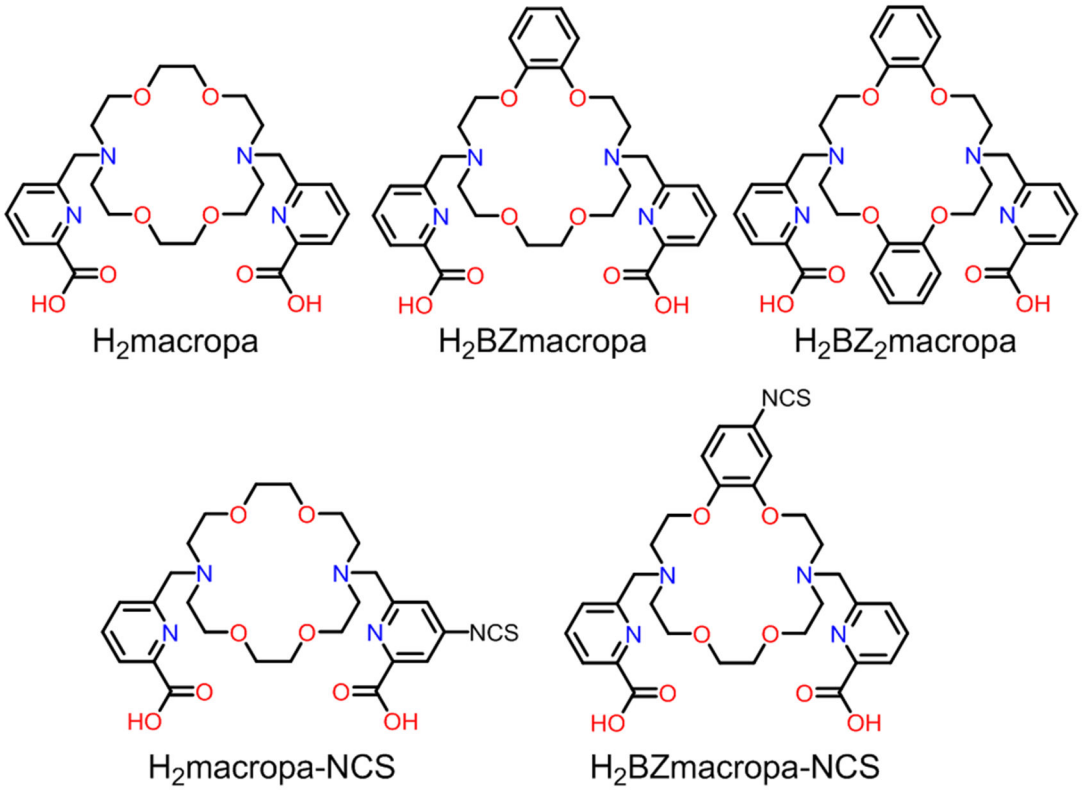

Chart 1.
Chelators Discussed in this Work.

Table 1.

Protonation Constants of Various Chelators and the Thermodynamic Stability Constants of Corresponding La^{3+} Complexes Determined by pH Potentiometry (25 °C and I = 0.1 M KCl).

	H_2macropa	H_2BZmacropa	H_2BZ_2macropa	H_4DOTA	H_5DTPA	H_4EDTA
log K_1	7.41(1)[c]	7.06(2)	6.89(7)	11.14[d]	10.45[e]	10.17[e]
log K_2	6.85(1)[c]	6.41(1)	6.11(3)	9.69[d]	8.53[e]	6.11[e]
log K_3	3.32(1)[c]	3.35(2)	3.36(3)	4.84[d]	4.28[e]	2.68[e]
log K_4	2.36(1)[c]	2.41(9)	2.26(9)	3.95[d]	2.65[e]	2.00[e]
log K_5	1.69(1)[c]		-		1.82[e]	1.5[e]
log K_{LaL}	**14.99(2)** [c]	**13.99(5)**	**12.04(6)**	**21.7(1)** [d]	**19.48** [e]	**15.46** [e]
log K_{LaHL}	**2.28(3)** [c]	-	-	**2.5(2)** [d]	-	**2.24** [e]
log K'_{La}[a]	14.63	13.81	11.92	15.67	15.27	12.67
pLa[b]	15.58	14.77	12.87	16.62	16.22	13.62

[a] Conditional stability constants (log K'_M) at pH 7.4, 25 °C, and I = 0.1 M KCl

[b] pM values calculated from $-\log [M]_{free}$ ($[M]_{total} = 10^{-6}$ M, $[L]_{total} = 10^{-5}$ M, pH 7.4, 25 °C, and I = 0.1 M KCl)

[c] 0.1 M KCl, ref [21].

[d] 0.1 M KCl, ref [22].

[e] 0.1 M, ref [23].